Supplement of Atmos. Chem. Phys., 17, 7495–7507, 2017
https://doi.org/10.5194/acp-17-7495-2017-supplement

Atmospheric Chemistry and Physics
Open Access
EGU

Supplement of

Experimental determination of Henry's law constants of difluoromethane (HFC-32) and the salting-out effects in aqueous salt solutions relevant to seawater

Shuzo Kutsuna

Correspondence to: Shuzo Kutsuna (s-kutsuna@aist.go.jp)

S1. Equilibrium time for the PRV-HS method experiments

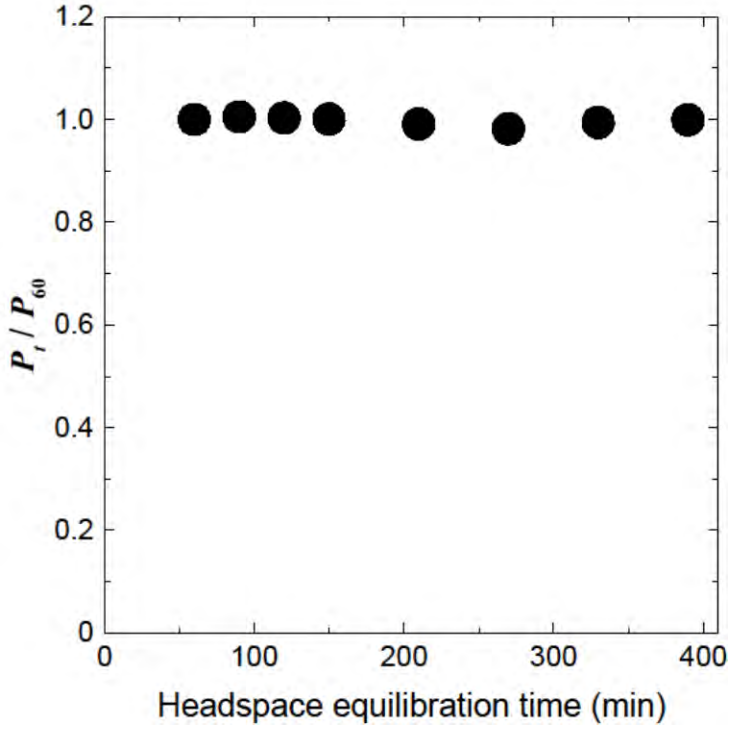

Figure S1. Relative areas of GC-MS peaks for CH_2F_2 versus headspace time duration for equilibration of 9.0 cm^3 of aqueous CH_2F_2 at 353 K.

S2. An example of the IGS method experiments

Figure S2 shows an example of time profile of P_t and how to calculate the k_1 value for the IGS method experiments. The k_1 value at each time was calculated by fitting nearest three data of P_t for each time. The average of the k_1 values is given as the k_1 value for the experimental run. Two standard deviation of the k_1 values gives errors of the k_1 value for the experimental run.

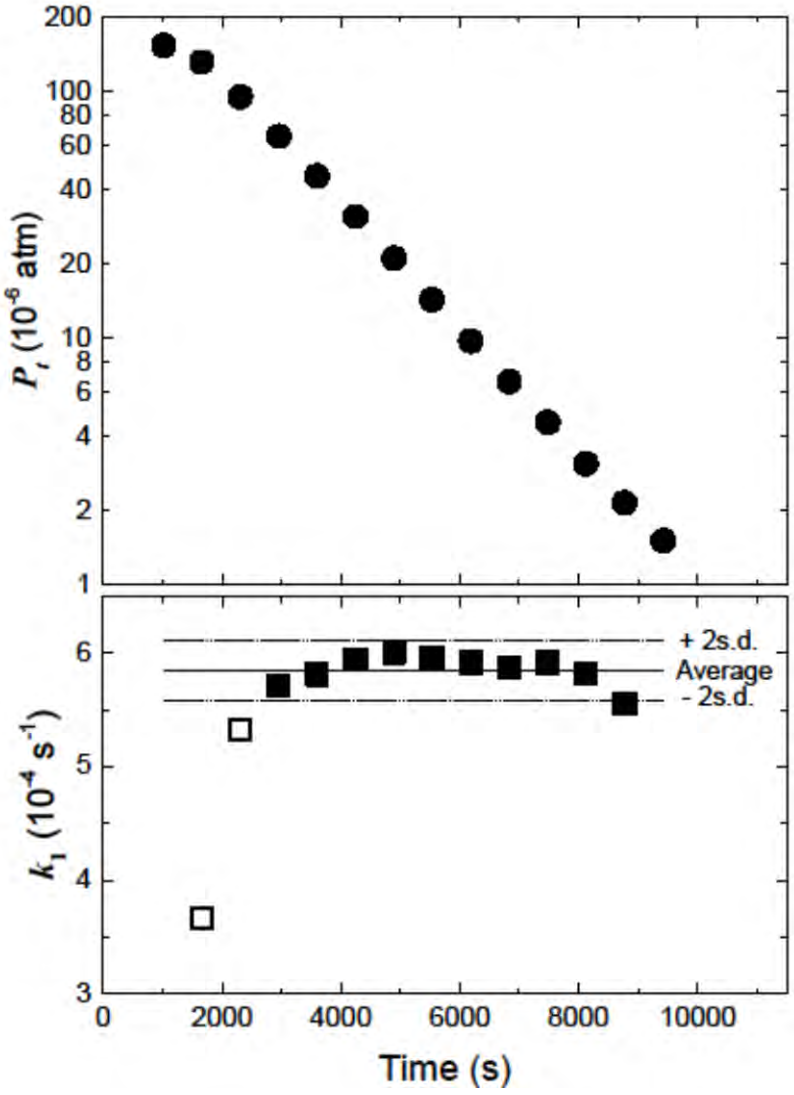

Figure S2. An IGS experimental result for V = 0.350 dm^3 and $F = 3.32\times10^{-4}$ dm^3 s^{-1} at 25°C. (upper panel) time profile of P_t; (lower panel) values of k_1 calculated by fitting nearest three data of P_t for each time with respect to Eq. (1).

S3. Results of the PRV-HS method experiments

Figure S3 illustrates the results of a PRV-HS experiment at 313 K. In panel A, peak area (S_{ij}) is plotted against the volume of the CH_2F_2 gas mixture added (v_j) for V_i = 9.0, 7.5, 6.0, 4.5, 3.0, and 1.5 cm^3. For each V_i, the data form a straight line intersecting the origin, indicating that S_{ij} is proportional to v_j for vials with the same value of V_i. The slope (L_i) of each line is obtained by linear regression with respect to Eq. (8), and the reciprocal of the slope (L_i^{-1}) is plotted against the phase ratio (V_i/V_0) in panel B of Fig. S3. Plots of L_i^{-1} and V_i/V_0 obey Eq. (9). Table S1 lists the values of L_i^{-1}, the slopes and the intercepts for linear regression with respect to Eq. (9), and the $K_H(T)$ values calculated from the slopes and the intercepts. Two measurements of $K_H(T)$ were carried out at each temperature.

Furthermore, the $K_H(T)$ values, along with errors of them at 95% confidence level, were also estimated by non-liner fitting of the two datasets simultaneously at each temperature by use of Eq. (11) (Fig. S4). The $K_H(T)$ values and their errors thus estimated are plotted in Fig. 2 and are listed in Table S1.

Table S1. L_i values for various V_i/V_0 ratios at various temperatures, slopes and intercepts for linear regression with respect to Eq. (10), $K_H(T)$ values calculated from the slopes and intercepts, and $K_H(T)$ values and the errors at 95% confidence level estimated by non-linear fitting the two datasets simultaneously at each temperature (Fig. S4) with respect to Eq. (11).

T	L_i (a.u.) [a]						Eq. (10)	Eq. (10)	K_H ($M\ atm^{-1}$)		
(K)	V_i/V = 0.421	0.351	0.280	0.210	0.140	0.070	Intercept	Slope	Eq. (10)	Eq. (11)[b, c]	Eq. (13)[b]
353	3.226±0.002	3.270±0.026	3.330±0.004	3.391±0.008	3.462±0.014	3.526±0.009	3.581	–0.870	0.026	0.027 ±0.002 (±0.003)	0.028 ±0.003
	2.044±0.006	2.050±0.012	2.112±0.010	2.132±0.009	2.186±0.021	2.209±0.011	2.248	–0.513	0.027		
343	3.000±0.018	3.025±0.009	3.070±0.008	3.089±0.015	3.117±0.015	3.148±0.018	3.179	–0.423	0.031	0.031 ±0.001 (±0.002)	0.031 ±0.002
	1.949±0.004	1.955±0.005	1.968±0.003	1.998±0.004	2.020±0.002	2.030±0.009	2.050	–0.258	0.031		
333	3.247±0.018	3.234±0.018	3.243±0.015	3.241±0.010	3.247±0.009	3.223±0.013	3.231	0.034	0.037	0.036 ±0.003 (±0.004)	0.035 ±0.002
	3.080±0.009	3.044±0.006	3.082±0.005	3.127±0.009	3.113±0.008	3.134±0.014	3.149	–0.213	0.034		
323	3.208±0.011	3.190±0.008	3.133±0.010	3.134±0.011	3.092±0.008	3.093±0.006	3.055	0.355	0.042	0.043 ±0.002 (±0.004)	0.040 ±0.001
	3.357±0.010	3.289±0.014	3.275±0.005	3.233±0.004	3.226±0.016	3.160±0.001	3.135	0.496	0.044		
313	3.245±0.018	3.185±0.013	3.100±0.015	3.022±0.012	2.995±0.012	2.915±0.011	2.848	0.935	0.052	0.052 ±0.003 (±0.005)	0.047 ±0.001
	2.162±0.031	2.134±0.010	2.060±0.014	2.029±0.018	1.992±0.010	1.925±0.018	1.896	0.612	0.052		

a. Errors are 2σ for the regression only.; b. Errors are those at 95% confidence level for the regression only.; c. Number in parenthesis represents both errors at 95% confidence level for the regression and potential systematic bias (±4%).

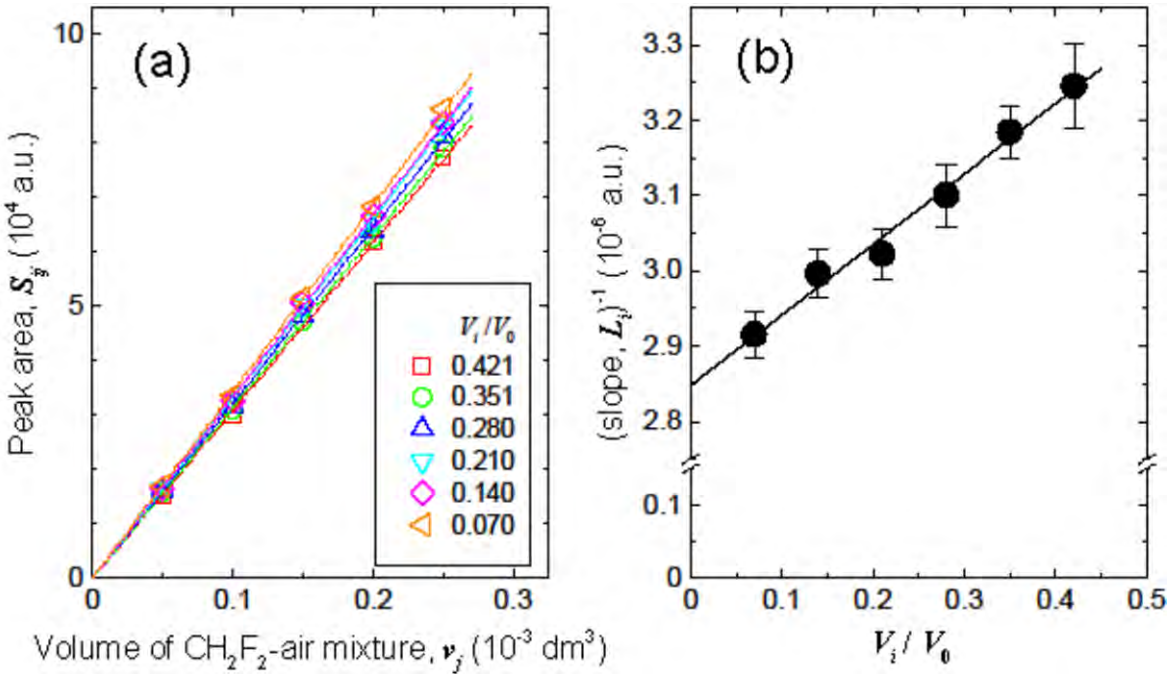

Figure S3. Headspace GC-MS measurements for six series of test samples containing water (V_i in cm^3) to which a CH_2F_2–air mixture was added (v_j in cm^3) at 313 K. (a) Plot of peak area (S_{ij}) versus v_j for test samples containing volume V_i of water. Slope (L_i) was obtained by linear fitting of the data to Eq. (8) for samples of the same V_i. (b) Plot of L_i^{-1} versus V_i/V_0 fitted to Eq. (10).

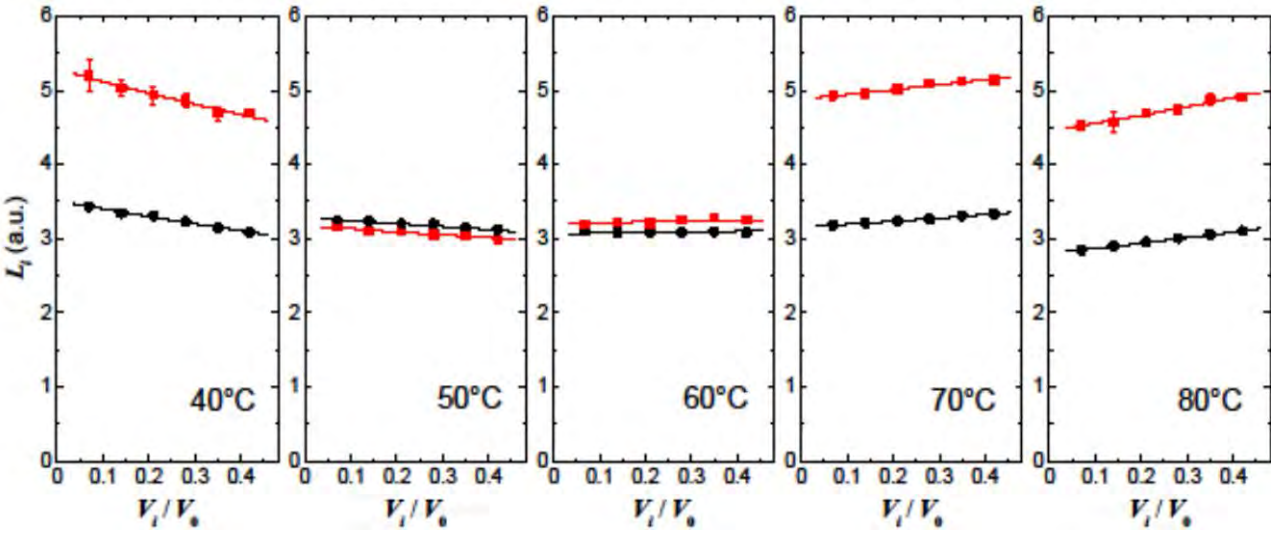

Figure S4. Plot of L_i versus V_i/V_0 for the PRV-HS measurements at each temperature. Bold curves represent the simultaneous fitting of the two datasets at each temperature by Eq. (11).

S4. Determination of salting-out effects in artificial seawater

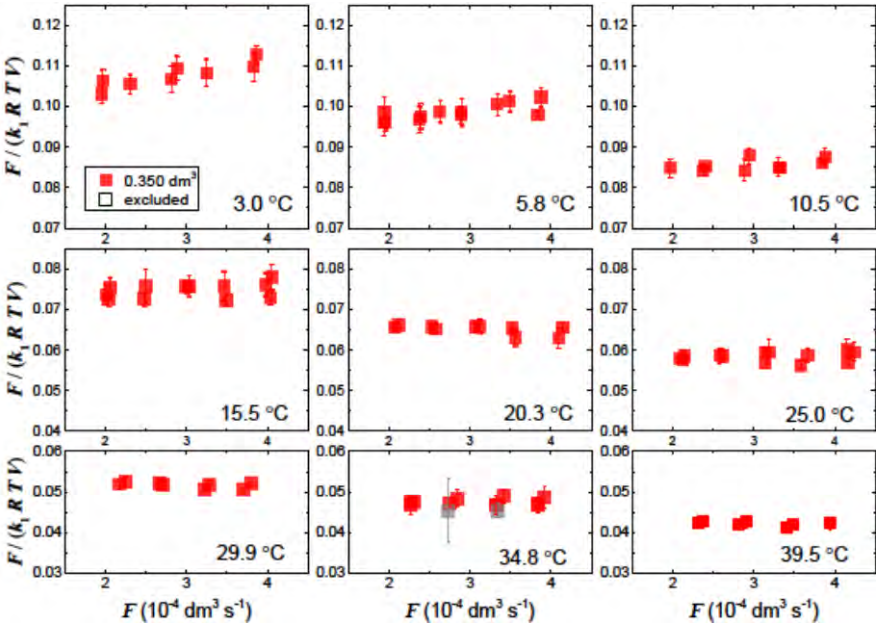

Figure S5. Plots of values of $F/(k_1RTV)$ against F at each temperature for 0.35 dm^3 of a-seawater at 4.452‰. Error bars represent 2σ due to errors of values of k_1 as described in Sect. S2. Grey symbols represent the data excluded for calculating the average.

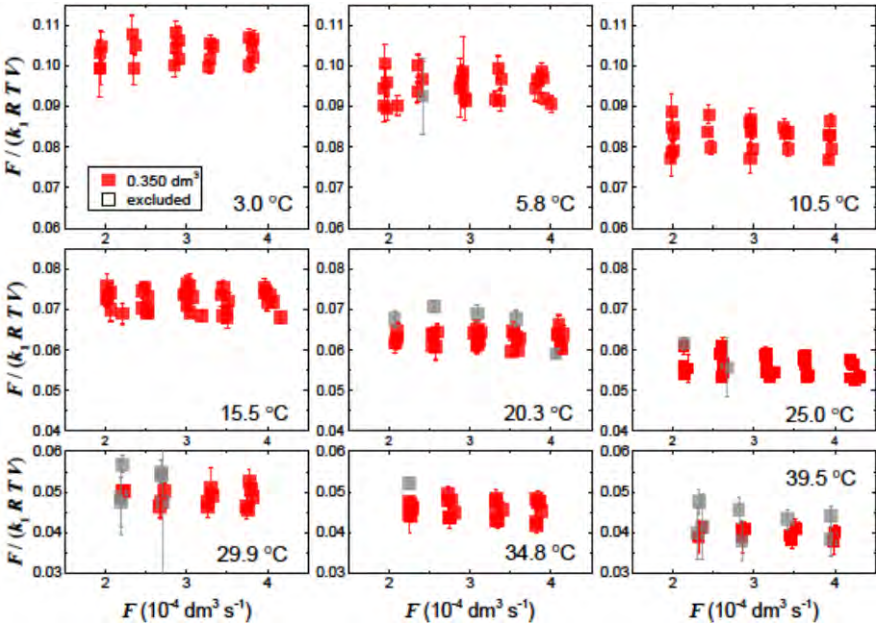

Figure S6. Plots of values of $F/(k_1RTV)$ against F at each temperature for 0.35 dm^3 of a-seawater at 8.921‰. Error bars represent 2σ due to errors of values of k_1 as described in Sect. S2. Grey symbols represent the data excluded for calculating the average.

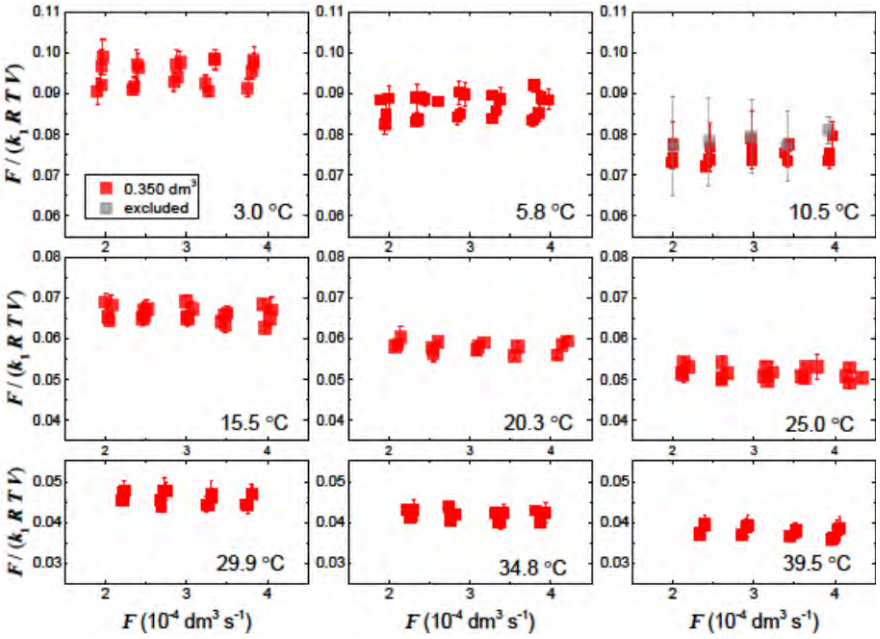

Figure S7. Plots of values of $F/(k_1RTV)$ against F at each temperature for 0.35 dm^3 of a-seawater at 21.520‰. Error bars represent 2σ due to errors of values of k_1 as described in Sect. S2. Grey symbols represent the data excluded for calculating the average.

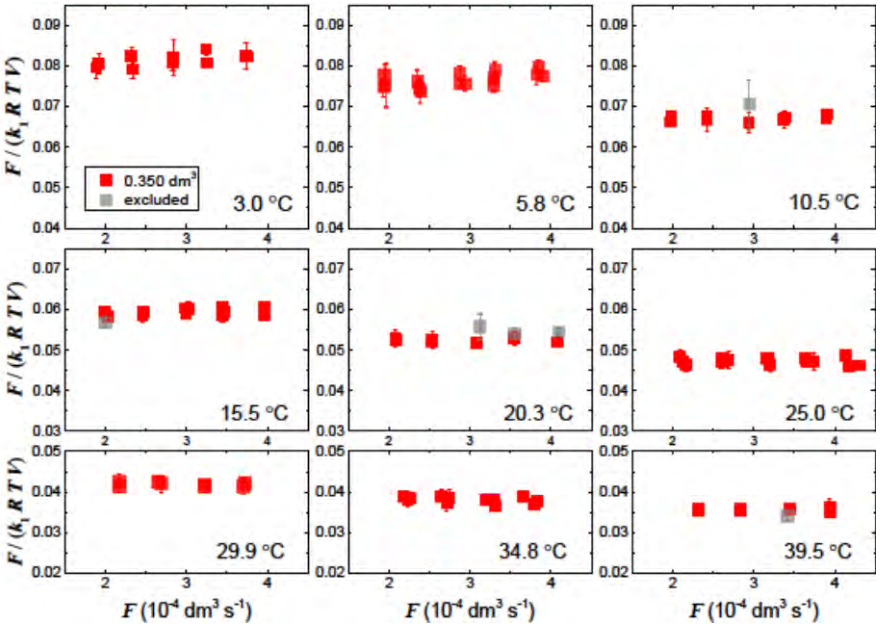

Figure S8. Plots of values of $F/(k_1RTV)$ against F at each temperature for 0.35 dm^3 of a-seawater at 51.534‰. Error bars represent 2σ due to errors of values of k_1 as described in Sect. S2. Grey symbols represent the data excluded for calculating the average.

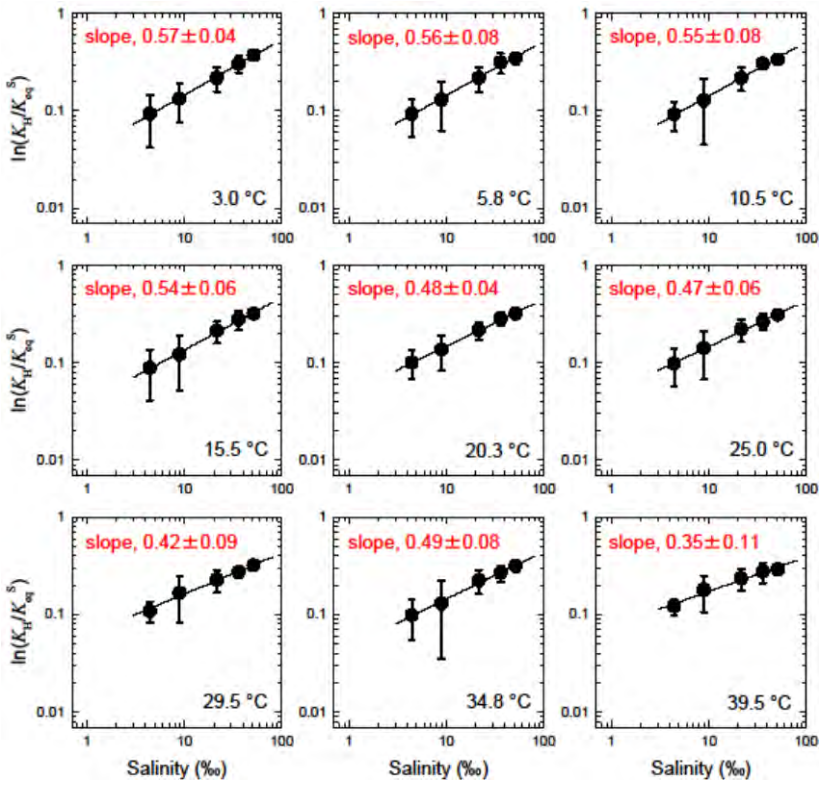

Figure S9. log-log plots for $\ln(K_H(T)/K_{eq}^S(T))$ vs. salinity in a-seawater at each temperature. Bold lines represent the fitting obtained by a liner regression. Errors are those at 95% confidence level for the regression only.

Table S2. Values of k_s (Eq. (17)) and comparison of values of K_{eq}^S calculated at each temperature by Eq. (17) with those by Eq. (22).

Temperature (°C)	k_s ($‰^{-1}$)	[K_{eq}^S from Eq. (17)]/ [K_{eq}^S from Eq. (22)] at 30‰	at 35‰	at 40‰	[K_{eq}^S at 30‰]/ [K_{eq}^S at 40‰] Eq. (17)	Eq. (22)
3.0	0.00811	1.027	1.008	0.988	1.084	1.043
5.8	0.00785	1.033	1.014	0.995	1.082	1.042
10.5	0.00768	1.033	1.016	0.997	1.080	1.042
15.5	0.00718	1.044	1.028	1.012	1.074	1.041
20.3	0.00728	1.037	1.020	1.003	1.076	1.040
25.0	0.00704	1.040	1.024	1.008	1.073	1.039
29.9	0.00731	1.027	1.010	0.992	1.076	1.039
34.8	0.00713	1.029	1.012	0.995	1.074	1.038
39.5	0.00709	1.026	1.010	0.992	1.073	1.038

S5. Discussion of potential reason for this salting-out effect of CH_2F_2 solubility in a-seawater (deviation from Sechenov relationship)

The reason that the salting-out effect of CH_2F_2 solubility in a-seawater depends on $S^{0.5}$ is not clear. Specific properties of CH_2F_2 –small molecular volume, which results in small work of cavity creation (Graziano, 2004; 2008), and large solute-solvent attractive potential energy in water and a-seawater− may cause deviation from Sechenov relationship. This possibility may be discussed here.

I calculate Ben-Naim standard Gibbs energy $\Delta G^{\bullet}$, enthalpy $\Delta H^{\bullet}$, and entropy $\Delta S^{\bullet}$ changes for dissolution of CH_2F_2 in water because these values correspond to the values for the transfer from a fixed position in the gas phase to a fixed position in water. Values of $\Delta G^{\bullet}$, $\Delta H^{\bullet}$, and $\Delta S^{\bullet}$ are calculated on the basis of the Ostwald solubility coefficient, $L(T)$, as follows.

$$\ln(L(T)) = \ln\left(RTK_{\mathrm{eq}}{}^{S}(T)\right) \quad \text{(B1)}$$

$$\Delta G^{\cdot} = R'T\ln(L(T)) \quad \text{(B2)}$$

$$\Delta H^{\cdot} = -\frac{\partial}{\partial(1/T)}\left(\frac{\Delta G^{\cdot}}{T}\right) \quad \text{(B3)}$$

$$\Delta S^{\cdot} = \frac{\Delta H^{\cdot} - \Delta G^{\cdot}}{T} \quad \text{(B4)}$$

where both R and R' represent gas constant but their units are different: R = 0.0821 in atm dm^3 K^{-1} mol^{-1}; R' = 8.314 in J K^{-1} mol^{-1}.

Combining Eqs. (B1), (B2), (B3), and (B4) with Eqs. (14) and (15), $\Delta G^{\bullet}$ (kJ mol^{-1}), $\Delta H^{\bullet}$ (kJ mol^{-1}), and $\Delta S^{\bullet}$ (J mol^{-1} K^{-1}) are represented by ΔG_{sol} and ΔH_{sol} as follows:

$$\Delta G^{\cdot} = \Delta G_{\mathrm{sol}} + R'T\ln(RT) \quad \text{(B5)}$$

$$\Delta H^{\cdot} = \Delta H_{\mathrm{sol}} + R'T \quad \text{(B6)}$$

$$\Delta S^{\cdot} = \frac{\Delta H_{\mathrm{sol}} - \Delta G_{\mathrm{sol}}}{T} + R' - R'\ln(RT) \quad \text{(B7)}$$

Values of $\Delta G^{\bullet}$, $\Delta H^{\bullet}$, and $\Delta S^{\bullet}$ calculated at 298 K are listed in Table S3. Table S3 also lists values of $\Delta G^{\bullet}$, $\Delta H^{\bullet}$, and $\Delta S^{\bullet}$ reported for CH_3F and C_2H_6 (Graziano, 2004) and CH_4 (Graziano, 2008) at 298 K. The chemicals, which having a methyl group, in Table S3 are classified into two groups (CH_2F_2 and CH_3F; CH_4 and C_2H_6) according to $\Delta G^{\bullet}$.

Table S3 lists values of ΔG_{c}, E_a and ΔH^h deduced using a scaled particle theory (Granziano, 2004; 2008). ΔG_c is the work of cavity creation to insert a solute in a solvent. E_a is a solute-solvent attractive potential energy and accounts for the solute-solvent interactions consisting of dispersion, dipole-induced dipole, and dipole-dipole contributions. ΔH^h is enthalpy of solvent molecules reorganization caused by solute insertion. The solvent reorganization mainly involves a rearrangement of H-bonds.

ΔG_{c} is entropic in nature in all liquids, being a measure of the excluded volume effect due to a reduction in the spatial configurations accessible to liquid molecules upon cavity creation. Hence, C_2H_6 has larger value of ΔG_{c} than CH_3F and CH_4. ΔG_{c}, E_a, and ΔH^h are related to $\Delta G^{\bullet}$ and $\Delta H^{\bullet}$ as follows (Graziano, 2008):

$$\Delta G^{\cdot} = \Delta G_c + E_a \quad \text{(B8)}$$

$$\Delta H^{\cdot} = E_a + \Delta H^h \quad \text{(B9)}$$

Table S3 thus suggests that smaller value of $\Delta G^{\cdot}$ of CH_3F than CH_4 is due to large solute-solvent attractive potential energy ($-E_a$) of CH_3F.

Table S3. Ben-Naim standard hydration Gibbs energy $\Delta G^{\cdot}$, enthalpy $\Delta H^{\cdot}$, and entropy $\Delta S^{\cdot}$ changes for dissolution of CH_2F_2 at 298 K determined here and the corresponding values and values of ΔG_c, E_a and ΔH^h reported for CH_3F and C_2H_6 (Granziano, 2004) and CH_4 (Graziano, 2008).

	$\Delta G^{\cdot}$ (kJ mol^{-1})	$\Delta H^{\cdot}$ (kJ mol^{-1})	$\Delta S^{\cdot}$ (J K^{-1} mol^{-1})	ΔG_c (kJ mol^{-1})	E_a (kJ mol^{-1})	ΔH^h (kJ mol^{-1})
CH_2F_2	−1.1	−14.7	−45.4			
CH_3F	−0.9	−15.8	−50.0	23.3	−24.3	8.5
CH_4	8.4	−10.9	−64.7	22.9	−14.5	3.7
C_2H_6	7.7	−17.5	−84.5	28.4	−20.7	3.2

Graziano (2008) definitively explained the salting-out of CH_4 by sodium chloride at molecular level on the basis of a scaled particle theory. He explained that ΔG_c increase was linearly related to the increase in the volume packing density of the solutions (ξ_3) with adding NaCl. Such an increase of ΔG_c is probably the case for salting-out of CH_2F_2 by a-seawater observed in this study. He also explained that E_a was linearly related to the increase in ξ_3 assuming that a fraction of the dipole-induced dipole attractions could be taken into account by the parameterization of the dispersion contribution.

I think the possibility that E_a may be nonlinearly related to the increase in ξ_3 because of dipole-dipole interaction between CH_2F_2 and solvents. Temperature dependence in Eq. (22) suggests that salting-out effect of CH_2F_2 by a-seawater is enthalpic. Eqs. (22) and (B9) thus suggests that the salting-out of CH_2F_2 is mostly related to change in E_a. CH_2F_2 has relatively small value of ΔG_c because of its small molecular volume compared to other chemicals such as C_2H_6. Accordingly, $\Delta G^{\cdot}$, that is, solubility of CH_2F_2 would depend on E_a rather than ΔG_c. Therefore, I think that specific properties of CH_2F_2 – small molecular volume, which results in small work of cavity creation (Graziano, 2004; 2008), and large solute-solvent attractive potential energy in water and a-seawater– may cause deviation from Sechenov relationship.

References

Graziano, G.: Case study of enthalpy–entropy noncompensation. Journal of Chemical Physics, 120, 4467-4471, doi: 10.1063/1.1644094, 2004.

Graziano, G.: Salting out of methane by sodium chloride: A scaled particle theory study. Journal of Chemical Physics, 129, 084506, doi: 10.1063/1.2972979, 2008.

S6. Estimated results (Sect. 3.3) for monthly amount of CH_2F_2 dissolved in the ocean mixed layer at solubility equilibrium with the atmospheric CH_2F_2 (1 patm) and the depth distribution of the CH_2F_2 dissolved in each semi-hemisphere

Table S4. Monthly amount of CH_2F_2 dissolved in the ocean mixed layer at solubility equilibrium with the atmospheric CH_2F_2 (partial pressure, 1 patm) and the depth distribution of the CH_2F_2 dissolved in the southern semi-hemisphere (90° S - 30° S).

	Amount (Gg patm^{-1})	Distribution of the amount of CH_2F_2 dissolved in the ocean mixed layer with respect to the ocean mixed layer depth (%)					
		10 - 100 m	100 - 200 m	200 - 300 m	300 - 400 m	400 - 500 m	500 - 600 m
January	0.0169	94.9	2.9	1.0	0.5	0.3	0.3
February	0.0201	92.1	3.6	2.9	1.0	0.3	0.0
March	0.0255	87.8	9.2	1.7	0.7	0.2	0.4
April	0.0338	66.5	31.8	1.1	0.2	0.1	0.2
May	0.0409	48.5	48.1	2.2	0.8	0.3	0.0
June	0.0510	26.8	62.7	8.0	1.7	0.8	0.1
July	0.0571	14.1	69.3	12.2	3.3	0.9	0.1
August	0.0640	8.5	65.8	17.0	6.2	2.3	0.2
September	0.0609	13.5	61.0	14.6	8.2	2.7	0.0
October	0.0504	24.7	58.6	12.1	2.9	1.4	0.3
November	0.0335	60.4	30.5	4.6	2.2	2.3	0.1
December	0.0196	95.1	4.3	0.4	0.2	0.0	0.0

Table S5. Monthly amount of CH_2F_2 dissolved in the ocean mixed layer at solubility equilibrium with the atmospheric CH_2F_2 (partial pressure, 1 patm) and the depth distribution of the CH_2F_2 dissolved in the southern semi-hemisphere (30° S - 0° S).

	Amount (Gg patm^{-1})	Distribution of the amount of CH_2F_2 dissolved in the ocean mixed layer with respect to the ocean mixed layer depth (%)					
		10 - 100 m	100 - 200 m	200 - 300 m	300 - 400 m	400 - 500 m	500 - 600 m
January	0.0084	99.6	0.4	0	0	0	0
February	0.0084	99.7	0.3	0	0	0	0
March	0.0089	100.0	0	0	0	0	0
April	0.0106	100.0	0	0	0	0	0
May	0.0131	100.0	0	0	0	0	0
June	0.0163	97.1	2.9	0	0	0	0
July	0.0189	80.1	19.9	0	0	0	0
August	0.0193	73.1	26.9	0	0	0	0
September	0.0165	82.2	17.8	0	0	0	0
October	0.0124	94.6	5.4	0	0	0	0
November	0.0097	99.9	0.1	0	0	0	0
December	0.0087	100.0	0	0	0	0	0

Table S6. Monthly amount of CH_2F_2 dissolved in the ocean mixed layer at solubility equilibrium with the atmospheric CH_2F_2 (partial pressure, 1 patm) and the depth distribution of the CH_2F_2 dissolved in the northern semi-hemisphere (0° N - 30° N).

	Amount (Gg $patm^{-1}$)	Distribution of the amount of CH_2F_2 dissolved in the ocean mixed layer with respect to the ocean mixed layer depth (%)					
		10 - 100 m	100 - 200 m	200 - 300 m	300 - 400 m	400 - 500 m	500 - 600 m
January	0.0132	96.4	3.6	0	0	0	0
February	0.0126	95.9	4.1	0	0	0	0
March	0.0107	98.7	1.3	0	0	0	0
April	0.0087	99.8	0.2	0	0	0	0
May	0.0079	100.0	0	0	0	0	0
June	0.0080	100.0	0	0	0	0	0
July	0.0084	100.0	0	0	0	0	0
August	0.0082	100.0	0	0	0	0	0
September	0.0080	100.0	0	0	0	0	0
October	0.0086	100.0	0	0	0	0	0
November	0.0100	100.0	0	0	0	0	0
December	0.0118	100.0	0	0	0	0	0

Table S7. Monthly amount of CH_2F_2 dissolved in the ocean mixed layer at solubility equilibrium with the atmospheric CH_2F_2 (partial pressure, 1 patm) and the depth distribution of the CH_2F_2 dissolved in the northern semi-hemisphere (30° N - 90° N).

	Amount (Gg $patm^{-1}$)	Distribution of the amount of CH_2F_2 dissolved in the ocean mixed layer with respect to the ocean mixed layer depth (%)					
		10 - 100 m	100 - 200 m	200 - 300 m	300 - 400 m	400 - 500 m	500 - 600 m
January	0.0205	41.3	50.1	7.0	1.4	0.2	0.0
February	0.0225	34.5	55.3	7.1	2.3	0.6	0.2
March	0.0208	49.7	42.3	4.9	1.7	0.7	0.6
April	0.0147	79.7	17.6	1.7	0.4	0.0	0.6
May	0.0081	90.1	9.9	0	0	0	0
June	0.0055	97.7	2.3	0	0	0	0
July	0.0045	96.6	3.4	0	0	0	0
August	0.0048	94.4	5.6	0	0	0	0
September	0.0059	97.7	2.3	0	0	0	0
October	0.0084	99.6	0.4	0	0	0	0
November	0.0121	89.6	10.4	0.1	0	0	0
December	0.0163	71.0	26.1	2.9	0	0	0